Influence of electro-magnetic boundary conditions onto the onset of dynamo action in laboratory experiments.

Raul Avalos-Zuniga, Franck Plunian, Agris Gailitis

Influence of electromagnetic boundary conditions onto the onset of dynamo action in laboratory experiments

Raul Avalos-Zuniga and Franck Plunian*
Laboratoires des Ecoulements Géophysiques et Industriels, Boîte Postale 53, 38041 Grenoble Cedex 9, France

Agris Gailitis
Institute of Physics, University of Latvia, LV-2169 Salaspils 1, Riga district, Latvia
(Received 5 February 2003; revised manuscript received 11 July 2003; published 24 December 2003)

We study the onset of dynamo action of the Riga and Karlsruhe experiments with the addition of an external wall, the electromagnetic properties of which are different from those of the fluid in motion. We consider a wall of different thickness, conductivity, and permeability. We also consider the case of a ferrofluid in motion.

DOI: 10.1103/PhysRevE.68.066307 PACS number(s): 47.65.+a

I. INTRODUCTION

A. Objectives

Two dynamo experiments have been successful so far, one in Riga (Latvia) [1,2] and one in Karlsruhe (Germany) [3]. Both experiments are complementary to each other in many respects. One is monocellular with a dynamo mechanism based on a laminar kinematic approach. The second is multicellular with scale separation between the flow and the magnetic field leading to an α effect as assumed in turbulent dynamos. The first one produces a time-dependent magnetic field (Hopf bifurcation) whereas the second one produces a stationary magnetic field (stationary bifurcation). Finally in both cases the theoretical predictions proved to be in very good agreement with the experimental results. This gives good confidence for further theoretical investigations, as is done in this paper.

We address questions about the influence of electromagnetic boundary conditions onto the onset of dynamo action. Suppose, for example, that an external layer of stagnant fluid is added around the main motion, as is done in Riga. Does it help for dynamo action? What happens if instead of a stagnant fluid the external layer is a highly conducting wall or a ferromagnetic wall (with a magnetic permeability larger than vacuum permeability)? At last, what is the influence onto the onset of dynamo action when a ferrofluid is used (assuming a homogeneous permeability throughout the fluid) as proposed recently [4]?

The answers to these questions are of high interest for the next generation of dynamo experiments which are under way [5,6]. Indeed, with concern for natural dynamos, these new generation experiments do not have a flow geometry as well optimized as the two previous ones. Then the volume of moving liquid metal necessary to get dynamo action is much larger. In fact, this volume may even be underestimated by the theoretical predictions usually based on crude approximations as laminarity of the flow. Then the possibility to add external walls or stagnant fluid around the experiment as well as the use of a ferrofluid could become essential.

*Electronic address: Franck.Plunian@hmg.inpg.fr. URL: http://legi.hmg.inpg.fr/~plunian

B. Geometries of Riga and Karlsruhe experiments

For both experiments the appropriate coordinates are cylindrical (r,θ,z). The Riga dynamo experiment [1] is composed of three coaxial cylinders of radii $r_0=0.125$ m, $R=0.215$ m, and $R+e=0.4$ m. The flow is helical in the inner cylinder, backward between the inner and the second cylinder [Fig. 1(a)]. There is stagnant fluid in the outer cylinder. The same fluid (liquid sodium) has been used in every part of the experiment. The height of the device is $H=2.91$ m.

The most essential piece of the Karlsruhe dynamo experiment [3] is a cylindrical container with both radius R and height H somewhat less than 1 m, through which liquid sodium is driven by external pumps. By means of a system of channels, constituting 52 ''spin generators,'' a helical motion is organized [Fig. 1(b)]. The flow pattern is of Roberts [7] type and an estimate of the self-excitation condition for this experimental device has been derived from a mean-field solution with an α effect assumed to be constant in the cylinder [8].

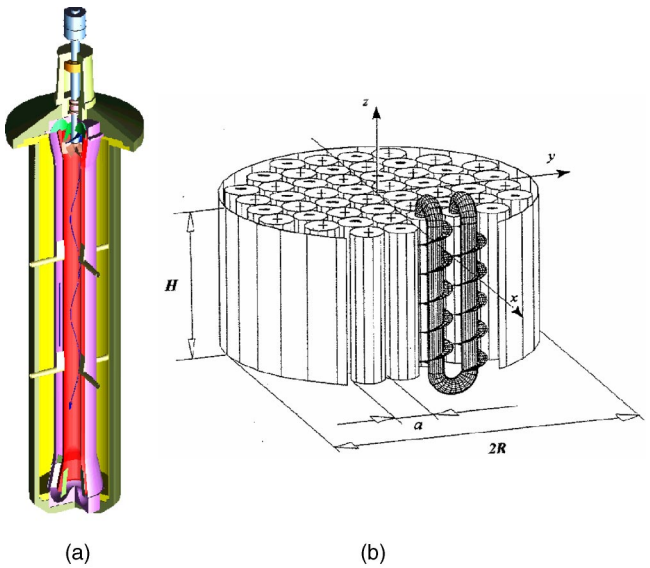

FIG. 1. The dynamo modules of the (a) Riga and (b) Karlsruhe experiments.

II. FORMULATION OF THE PROBLEM

A. Parameters

For our calculations we consider three coaxial cylindrical regions defined by their radii ($r_1=R$, $r_2=R+e$, $r_3=\infty$), their conductivities ($\sigma_1,\sigma_2,\sigma_3$), and permeabilities ($\mu_1,\mu_2,\mu_3$). Region 1 contains the moving fluid, region 2 is the conducting wall (or stagnant surrounding fluid), and region 3 is the insulator around the experiment ($\sigma_3=0$). However, for the sake of generality, we will replace σ_3 by zero only in the numerical applications.

B. Kinematic dynamo problem

As we are interested in the onset of the dynamo instability, it is sufficient to solve the kinematic dynamo problem in which the flow is considered as given. The magnetic field **B** must satisfy the induction equation and the divergence-free condition

$$\frac{\partial \mathbf{B}}{\partial t}=\boldsymbol{\nabla}\times(\mathbf{U}\times\mathbf{B})-\boldsymbol{\nabla}\times([\alpha]\mathbf{B})+(\mu\sigma)^{-1}\nabla^2\mathbf{B}, \tag{1}$$

$$\boldsymbol{\nabla}\cdot\mathbf{B}=0, \tag{2}$$

with appropriate boundary conditions (as we shall see later) and where the velocity field **U** and the $[\alpha]$ tensor may be nonzero only in region 1. The $[\alpha]$ tensor corresponds to a mean electromotive force which is linear and homogeneous in **B**. In that case the quantities **B** and **U** must be understood as mean quantities [9].

C. Velocity and $[\alpha]$ tensor

In the Riga experiment the velocity **U** is defined by $\mathbf{U}_0=(0,\omega r,\chi\omega r_0)$ for $r\leqslant r_0$ and $\mathbf{U}_1=(0,0,-\chi\omega r_0/(R/r_0)^2-1)$ for $r_0<r\leqslant r_1$. Therefore it is convenient to introduce an additional cylindrical region 0 defined by its radius $r=r_0$ distinct from region 1 ($r_0<r\leqslant r_1$) by its velocity but common by its conductivity $\sigma_0=\sigma_1$ and permeability $\mu_0=\mu_1$ (as it is the same fluid). The $[\alpha]$ tensor is identically zero at first order for the Riga experiment. Indeed, the currents induced by the small scale of the turbulence are negligible compared to the currents induced by the mean flow.

For the Karlsruhe experiment, it is the mean flow **U** which is zero. In that case, the $[\alpha]$ tensor writes $\alpha_{ij}=\alpha_\perp(\delta_{ij}-e_ie_j)$. This corresponds to an anisotropic α effect deduced from the symmetry properties of the flow. In addition, in the calculation of the mean electromotive force we neglected the contribution which contains the derivatives of **B**. This approximation leads to an error of about 10% on the instability threshold prediction [8,10]. However, this approximation is accurate enough for our present purpose.

For convenience we denote each region by l (=1, 2, or 3 plus the additional region $l=0$ for the Riga experiment).

D. Magnetic field

As the flow in both problems is z independent, axisymmetric, and time independent, a particular solution of Eq. (1) takes the form

$$\hat{\mathbf{B}}(r,\theta,z,t)=\mathbf{b}(r)\quad e^{pt+im\theta+ikz}, \tag{3}$$

p being the complex growth rate, m and k the azimuthal and vertical wave numbers. The superposition of all the (m,k) modes $\hat{\mathbf{B}}$ leads to the general solution **B** of Eq. (1) to which the boundary conditions apply.

The radial boundary conditions write $\lim_{r\to\infty}\mathbf{b}_3=\mathbf{0}$ plus the appropriate relations between each region l (see below). As these relations are satisfied by each particular solution $\hat{\mathbf{B}}$, they are also satisfied by **B**.

The axial boundary conditions write

$$\lim_{z\to\pm\infty}\mathbf{B}=\mathbf{0}, \tag{4}$$

$$(\boldsymbol{\nabla}\times\mathbf{B})_z=\mathbf{0}\ \text{ at }\quad z=\pm H/2. \tag{5}$$

Equation (5) means that there is no axial current crossing the insulating borders at both ends. In order to simplify the calculations, we shall consider only two (m,k) modes $\hat{\mathbf{B}}$, the superposition of which satisfies Eq. (5) only, as explained later in the paper.

III. METHOD OF SOLUTION

A. Solutions of the dynamo problem

By replacing Eq. (3) in Eq. (1) we find that in each region l the radial and azimuthal components of **b** must satisfy

$$\mathbf{b}_l''+\frac{1}{r}\mathbf{b}_l'+[A]\mathbf{b}_l=\mathbf{0} \tag{6}$$

with the prime denoting the r derivative and where the matrix A simply relates the different components of $\mathbf{b}_l$ in the induction equation. The A coefficients write

$$A_{11}=A_{22}=-\left(k^2+\frac{p}{\eta_l}+\frac{m^2+1}{r^2}+i\frac{m\omega_l+kV_l}{\eta_l}\right)$$

and $A_{12}=-A_{21}=-i(2m/r^2+k\alpha_l/\eta_l)$, with $\eta_l=(\sigma_l\mu_l)^{-1}$ and where α_l, ω_l, and V_l, are the magnetic diffusivity, the α effect, the rotation rate, and the z component of the velocity field appropriate to each region l and to each case (Riga or Karlsruhe) as defined above. Finally, the component b_{lz} can be determined subsequently by

$$b_{lz}=\frac{i}{k}\left(\frac{b_{lr}+imb_{l\theta}}{r}+b_{lr}'\right). \tag{7}$$

To find the solutions in the region l, instead of $(b_{lr},b_{l\theta})$ we look for $(b_{lr}+ib_{l\theta},b_{lr}-ib_{l\theta})$. These solutions can be written as a linear combination of modified Bessel's functions $I_{m+1}(\omega_l^+r)$ and $K_{m+1}(\omega_l^+r)$ for $b_{lr}+ib_{l\theta}$ and $I_{m-1}(\omega_l^-r)$ and $K_{m-1}(\omega_l^-r)$ for $b_{lr}-ib_{l\theta}$, where

$$(\omega_l^\pm)^2=k^2+\frac{p\pm\alpha_lk+i(m\omega_l+kV_l)}{\eta_l}. \tag{8}$$

In each region the solutions write in the form

$$(b_{lr}, ib_{l\theta}) = [F_l^+ I_{m+1}(\omega_l^+ r) + G_l^+ K_{m+1}(\omega_l^+ r)](1,1) + [F_l^- I_{m-1}(\omega_l^- r) + G_l^- K_{m-1}(\omega_l^- r)](1,-1), \tag{9}$$

where F_l^+, F_l^-, G_l^+, and G_l^- are constants. The regularity conditions for $r=0$ lead to $G_0^+ = G_0^- = 0$ for the Riga experiment and $G_1^+ = G_1^- = 0$ for the Karlsruhe experiment. The condition $\mathbf{b}_3 \to 0$ when $r \to \infty$ leads to $F_3^+ = F_3^- = 0$ for both experiments.

B. Radial boundary conditions

The normal component of **B**, the tangential component of $\mathbf{B}/\mu$, and the z component of the electric field $E_z = \eta(\nabla \times \mathbf{B})_z$ are continuous across each interface $r=r_0$ (only for Riga), $r=r_1$, and $r=r_2$. We can show that this set of relations is sufficient to describe all the radial boundary conditions of the problem. They write at $r=r_l$:

$$b_{l,r} = b_{l+1,r},$$

$$\frac{b_{l,\theta}}{\mu_l} = \frac{b_{l+1,\theta}}{\mu_{l+1}},$$

$$\frac{1}{\mu_l}\left(\frac{b_{l,r}}{r_l} + b'_{l,r}\right) = \frac{1}{\mu_{l+1}}\left(\frac{b_{l+1,r}}{r_l} + b'_{l+1,r}\right),$$

$$\eta_l\left(\frac{b_{l,\theta} - imb_{l,r}}{r_l} + b'_{l,\theta}\right) = \eta_{l+1}\left(\frac{b_{l+1,\theta} - imb_{l+1,r}}{r_l} + b'_{l+1,\theta}\right) \tag{10}$$

but for the Riga experiment at $r=r_0$ the last equation in Eq. (10) is replaced by

$$(b'_{1\theta}) = \left(b'_{0\theta} + \frac{1}{\eta_1}\omega r_0 b_{0r}\right). \tag{11}$$

C. Dispersion relation and dimensionless parameters

Replacing Eq. (9) into Eqs. (10) and (11), we find a system of eight equations for the Karlsruhe dynamo and twelve for the Riga dynamo. We have a nontrivial solution only if the determinant of the system is equal to zero. This writes in the form

$$F[R_m(\text{or } R_\alpha), k, p, m, \text{ geometric parameters}] = 0, \tag{12}$$

where R_m and R_α are magnetic Reynolds numbers defined by $R_m = \sigma_1 \mu_1 |\mathbf{U}_0|_{max} r_0$ for the Riga dynamo and $R_\alpha = \sigma_1 \mu_1 \alpha_\perp R$ for the Karlsruhe dynamo.

For the calculations we set $\sigma_3 = 0$ and define $\sigma_2/\sigma_1 = s$, $\mu_1/\mu_3 = q$, and $\mu_2/\mu_3 = n$. The dynamo onset corresponds to $\mathrm{Re}(p) = 0$ for which a critical R_m or R_α is calculated for different values of the parameters e/R, s, q, n, and for values of k chosen to satisfy the axial boundary condition (5) as explained below. Like any transcendental equation (Bessel functions with complex arguments), Eq. (12) has an infinite number of complex roots. It has to be solved numerically.

D. Treatment of the axial boundary condition

1. Method

Any (m,k) mode $\hat{\mathbf{B}}$ satisfying Eq. (12) automatically satisfies the radial boundary conditions but not the axial boundary condition. For that, again, one should write **B** as the superposition of an infinite number of particular solutions $\hat{\mathbf{B}}$ satisfying Eq. (12) and then apply Eqs. (4) and (5) to **B**. This is quite tedious and numerically demanding. Instead we look for an approximate solution **B** written as the superposition of only two particular solutions $\hat{\mathbf{B}}_1$ and $\hat{\mathbf{B}}_2$ which have the same growth rate p and with wave numbers k_1 and k_2, the difference of which writes

$$k_1 - k_2 = 2\pi/H. \tag{13}$$

If, in addition, both solutions have the same radial profile then Eq. (5) is satisfied, which is a good enough approximation of the actual experiments. Such an approximation is quite well justified for the Riga experiment because of its extended shape $H/R \sim 15$. Indeed, as the radial profile difference between both solutions at $z = \pm H/2$ is of the order $O(R/H)$, the boundary conditions (10) and (11) are satisfied with an error also of $O(R/H)$ and the parameters in Eq. (12) are obtained with an error of the order $O(R^2/H^2)$. In the case of Karlsruhe $(H/R \sim 1)$, the only justification is the common experience that in many similar cases replacing zero boundary conditions at infinity by periodic boundary conditions at both ends [leading to Eq. (12)] makes no crucial difference.

2. Karlsruhe

With such an approximation the problem is straightforward to solve for the Karlsruhe experiment. Indeed, as the flow pattern is symmetric to the plane $z=0$, after Eq. (12) the two solutions with $k = \pm \pi/H$ have the same p and satisfy Eq. (13). The clockwise and anticlockwise rotations are compensated, implying that the generated field pattern does not rotate around the symmetry axis. Hence Eq. (12) can be written in real variables, the growth rate p is real, and the field is stationary. Another way to understand it is that the α effect does not depend on z and therefore there is no preferred sense in the z direction for a magnetic wave to travel as it would be if the field is not stationary. Then the only thing which remains to do is solving Eq. (12) in order to find the critical R_α for which $p=0$. For the calculation we took $H/R = 1$.

3. Riga

For the Riga experiment the calculation is more complicated than for Karlsruhe for at least two reasons. First, the inner flow $(r < r_0)$ is helical and has then a preferred direction given by the rotation axis. Then any generated field pattern rotates round the vertical axis of symmetry. Hence the field is not stationary and the growth rate p is always complex. Second, one does not obtain the same result when V_z is replaced by $-V_z$ in both regions 0 and 1. This implies that $p(-k)$ is always different from $p(k)$ contrary to the

Karlsruhe case. As a result, for a given R_m one must look for two complex values of k which only differ from their real parts while their imaginary parts are equal (see Ref. [11] for more details) and which must satisfy Eqs. (12), (13), and $p(k_1,R_m)=p(k_2,R_m)$. The generated instability is usually known as absolute or global instability. The generated magnetic field $\mathbf{B}=\hat{\mathbf{B}}_1+\hat{\mathbf{B}}_2$ is a deformed [as $\Im(k_1)=\Im(k_2)\neq 0$] standing wave damped at both ends of the device and rotating around the symmetry axis. We call absolute critical R_m the value of R_m such that these conditions plus the additional relation $\mathrm{Re}(p)(k_1,R_m)=\mathrm{Re}(p)(k_2,R_m)=0$ are satisfied. At the time when the Riga experiment was designed, this method had already been used. In particular, the size r_1-r_0 of the Riga experiment was determined to lower the group velocity $v_G=i\partial p/\partial k$ of the above mentioned absolute instability. For our calculations we used the values of r_0, $r_1(=R)$ and H as given above and $\chi=1$ which is representative of the actual flow of the Riga experiment [1].

IV. RESULTS

A. Integral quantities

In all our calculations for both Riga and Karlsruhe the azimuthal mode $m=1$ has always been found to be dominant. Therefore in the rest of the paper only the results for this mode are presented. From now R_m (R_α) denotes the absolute critical R_m (critical R_α). In order to give some physical justification of our results we need to define the following additional quantities $\mathcal{W}_l$, $\mathcal{P}_l$, $\mathcal{J}_l$, and $\mathcal{S}_l$ which are, respectively, the magnetic energy, the Poynting flux, the Joule dissipation, and the work of the Lorenz forces in the region Ω_l ($l=1$ for the fluid, $l=2$ for the wall, and $l=3$ for the vacuum). They are defined by

$$\mathcal{W}_l=\int_{(\Omega_l)}\frac{B^2}{2\mu}d\Omega,\mathcal{P}_l=\int_{(S_l)}\left(\frac{\mathbf{B}}{\mu}\times\mathbf{E}\right)\cdot\mathbf{n}dS, \tag{14}$$

$$\mathcal{J}_l=\int_{(\Omega_l)}\frac{j^2}{\sigma}d\Omega,\mathcal{S}_l=\int_{(\Omega_l)}\mathbf{j}\cdot\mathcal{E}d\Omega, \tag{15}$$

where $\mathcal{E}=\mathbf{U}\times\mathbf{B}$ for Riga and $\mathcal{E}=-[\alpha]\mathbf{B}$ for Karlsruhe. The region (Ω_l) is delimited by the boundary(ies) (S_l) of normal $\mathbf{n}$ and $\mathbf{j}=\boldsymbol{\nabla}\times\mathbf{B}/\mu$ is the current density. Multiplying Eq. (1) by $\mathbf{B}/\mu$ and integrating in each region l we find

$$\frac{\partial\mathcal{W}_1}{\partial t}=\mathcal{P}_1+\mathcal{S}_1-\mathcal{J}_1,\quad \frac{\partial\mathcal{W}_2}{\partial t}=\mathcal{P}_2-\mathcal{J}_2, \tag{16}$$

$$\frac{\partial\mathcal{W}_3}{\partial t}=\mathcal{P}_3,\quad \mathcal{P}_1+\mathcal{P}_2+\mathcal{P}_3=0. \tag{17}$$

Dynamo action corresponds to

$$\mathcal{S}_1\geqslant\mathcal{J}_1+\mathcal{J}_2 \tag{18}$$

with the equal sign for the instability threshold. It means that at the threshold the work of the Lorenz forces $\mathcal{S}_1$ must compensate the total ohmic dissipation.

B. Rigid body helical flow

Before dealing with the Riga and Karlsruhe experiments we first want to mention results for the academic case of a rigid body helical flow surrounded by a conducting wall, both having infinite height. This case corresponds to have $r_0=R$ in our calculations for the Riga geometry (in that case region 1 of the backward flow does not exist). However, instead of looking for an absolute instability, as for Riga, we simply look for the onset of the dynamo instability corresponding to the minimum value of R_m for a given k. This instability is found to be of convective type, any primordial magnetic perturbation when growing being also traveling along the axis of symmetry of the flow.

We repeated the results of Ref. [12] on the dependence on conductivity and thickness. A decrease of the dynamo threshold has been found as the dimensionless wall thickness e/R or wall conductivity s was increased. The usual picture to explain this result is that increasing the wall thickness or wall conductivity leads in both cases to a reduction of the ohmic dissipation. From Eq. (18) the reduction of the total dissipation $\mathcal{J}_1+\mathcal{J}_2$ is equivalent to the reduction of $\mathcal{S}_1$, which is directly related to the threshold.

In the case of uniform conductivity $s=1$, it has been shown [13] that this picture is incomplete when the magnetic field is time dependent. In that case some additional eddy currents may be induced in the wall, increasing the ohmic dissipation. As a result, the dynamo threshold versus the wall thickness has a minimum.

In our calculations we checked out the existence of this minimum. We found that this effect is even more important for $s>1$. We found a similar effect for Riga as explained in the following section.

C. Influence of the wall conductivity

1. Threshold reduction rate

To present our results we adopt the point of view of any experimenter who wants to know how much reduction of the dynamo threshold he can obtain varying the wall thickness and conductivity, relatively to the case with no wall at all ($e=0$). For that we define a threshold reduction rate by

$$\Gamma=1-\frac{R_m(s,e/R)}{R_m(e=0)} \tag{19}$$

for Riga which also applies to Karlsruhe replacing R_m by R_α. We found $R_m(e=0)=41.16$ for Riga and $R_\alpha(e=0)=4.8$ for Karlsruhe. The reduction rates for Riga and Karlsruhe are plotted, respectively, in Fig. 2 and Fig. 3 versus s for $n=q=1$ and for different wall dimensionless thicknesses e/R.

In both cases Γ is always positive, which stresses the interest of having a conducting wall. Of course $\lim_{s\to 0}\Gamma=0$. Indeed, as the wall is surrounded by the vacuum, having a nonconducting wall is equivalent to having no wall at all. In both cases $\lim_{s\to\infty}\Gamma\approx 20\%$.

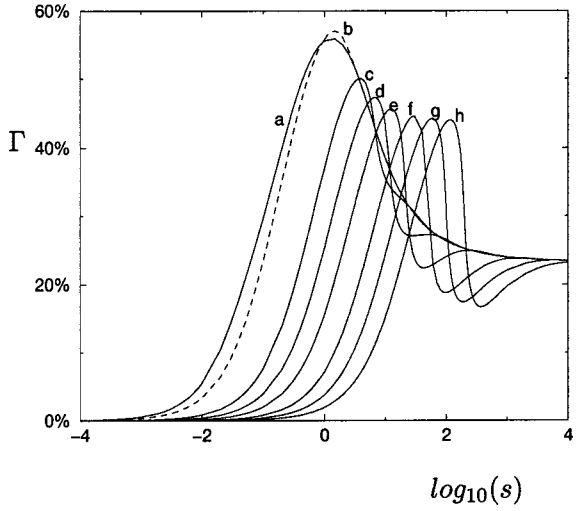

FIG. 2. Riga: The threshold reduction rate Γ vs $\log_{10}(s)$ for $n=q=1$ and different values of e/R. For curve (a) the ratio e/R is infinite, for (b) 86% (dashed line), for (c) 20%, for (d) 10%, for (e) 5%, for (f) 2%, for (g) 1%, and for (h) 0.5%.

2. The particular case $s=1$ for Riga

For $\log_{10}(s)=0$, the maximum reduction rate obtained for Riga is 55.9%. This is surprisingly close to the value obtained for a spherical dynamo model surrounded by a quiescent conducting external shell considered in Ref. [14]. In Table 8 of Ref. [14], they found $R_m(e=0)=3901.11$ and $R_m(e=\infty)=1659.05$ leading to $\Gamma=57.5\%$.

A remarkable point for Riga is that the choice adopted for the experiment, $e/R=86\%$ (curve b) and $s=1$, leads to the maximum threshold reduction rate. This shows that there is no benefit of adding a high electroconducting wall instead of an outer stagnant layer of fluid.

In Fig. 2 the dashed curve (b) goes above the solid curve (a) for $s=O(1)$. This shows that there is a wall thickness ($\approx 86\%$ for Riga) for which the dissipation is minimum. For a larger thickness (curve a) additional dissipation occurs, probably because of additional eddy currents as found in Ref. [13] for the rigid body helical flow. We recall here that this effect is related to the time dependency of the solution. This would explain why such a curves crossing is observed for Riga (time-dependent solution) and not for Karlsruhe (stationary solution).

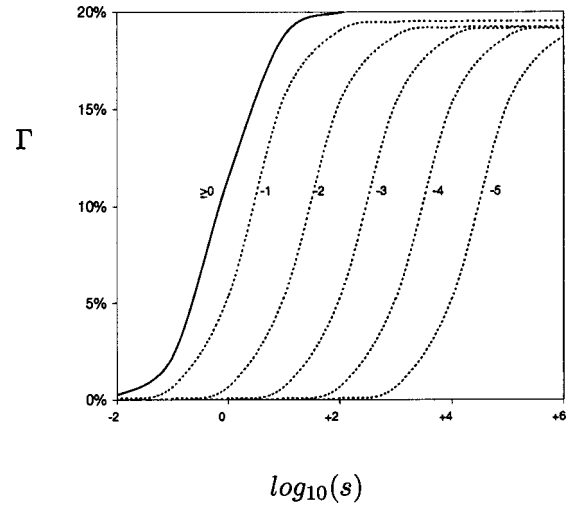

FIG. 3. Karlsruhe: The threshold reduction rate Γ vs $\log_{10}(s)$ for $n=q=1$. The labels indicate $\log_{10}(e/R)$.

3. Physical interpretation

In this section we give some physical interpretation on the behavior of Γ versus s. In a first step let us consider the case of Karlsruhe for which Γ increases monotonically with s. From Eq. (18) the threshold is directly related to $\mathcal{J}_1$ and $\mathcal{J}_2$ the dissipation in the fluid and the wall. We first show that in both cases $s\ll 1$ or $s\gg 1$ we have $\mathcal{J}_2\ll\mathcal{J}_1$.

For $s\ll 1$ the electric currents circulate mainly in the fluid. At the fluid-wall boundary we have $j_1\approx j_{t1}$ and $j_2\approx j_{t2}$ where the subscript t denotes the tangential component. Writing the continuity of the tangential component of the electric field across the fluid-wall boundary we find that $j_{t1}\sim j_{t2}/s$. Then integrating on both regions (fluid and wall) we find that $\mathcal{J}_1\approx R^2 j_{t1}^2/\sigma_1$ and that $\mathcal{J}_2\approx Re' j_{t2}^2/\sigma_2$ with $e'=eR/(R+e)$. Indeed when $e\gg R$ it is reasonable to assume that the currents in the wall close within a distance R (instead of e) from the fluid-wall boundary. As a result we find that $\mathcal{J}_2/\mathcal{J}_1=O(se'/R)$.

For $s\gg 1$ the current lines in the fluid at the fluid-wall boundary are mainly perpendicular to the boundary. Therefore we have $j_1\approx j_{n1}$ where the subscript n denotes the normal component, and again $j_2\approx j_{t2}$ as the currents have to close up in the wall. So we find that $\mathcal{J}_1\approx R^2 j_{n1}^2/\sigma_1$ and that $\mathcal{J}_2\approx Re' j_{t2}^2/\sigma_2$. Now from the definition of the current density $\mathbf{j}=\boldsymbol{\nabla}\times\mathbf{B}/\mu$ we can approximate $j_{t2}\approx B_{t2}/e'\mu_2$. Writing the continuity of B_t/μ across the fluid-wall boundary we find that $\mathcal{J}_2/\mathcal{J}_1=O(R/se')$.

So we can conclude that for $se'/R\ll 1$ or $se'/R\gg 1$, the ohmic dissipation is mainly concentrated in the fluid. Therefore from Eq. (18) the threshold is directly related to the ohmic dissipation in the fluid. The main difference between both limits $se'/R\ll 1$ and $se'/R\gg 1$ is the change of geometry of the current lines in the fluid.

For $se'/R\ll 1$ the current lines are constrained to close up mainly in the fluid whereas for $se'/R\gg 1$ the current lines in the fluid are perpendicular to the wall. Therefore the current lines are tighter for $se'/R\ll 1$ than for $se'/R\gg 1$. Consequently we understand why the dissipation is the largest when $se'/R\ll 1$ and that Γ increases with s. Now if our argument is correct this change of geometry of the current lines should occur at the transition between the two previous limits, namely, for $se'/R=O(1)$. In order to check this out we plot Γ versus se'/R in Fig. 4. We find that all the curves for Karlsruhe merge pretty well (dotted curves at the bottom) and that their change of curvature occurs indeed for $se'/R=O(1)$.

As a second step we consider the case of Riga for which some additional eddy currents must be considered leading to an enhanced dissipation $\mathcal{J}_2$ concentrated in the wall. Now following the same arguments as for the stationary case, namely, that as $\mathcal{J}_2/\mathcal{J}_1$ is maximum for $se'/R=O(1)$, we

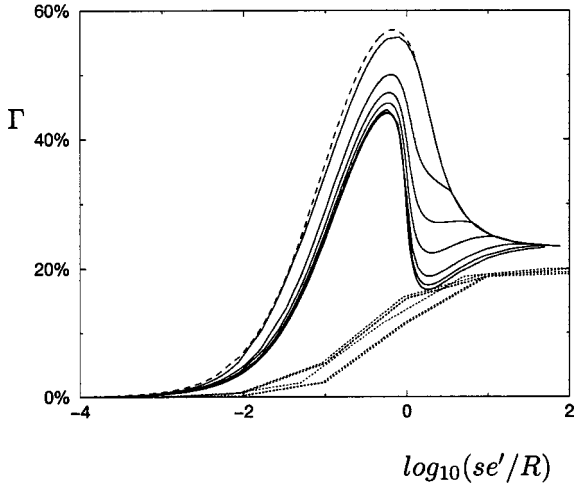

FIG. 4. Threshold reduction rate Γ vs $\log_{10}(se'/R)$ for $n=q=1$ and different values of e/R. The solid (dotted) curves in the upper (lower) part correspond to Riga (Karlsruhe). The dashed curve corresponds again to curve b of Fig. 2.

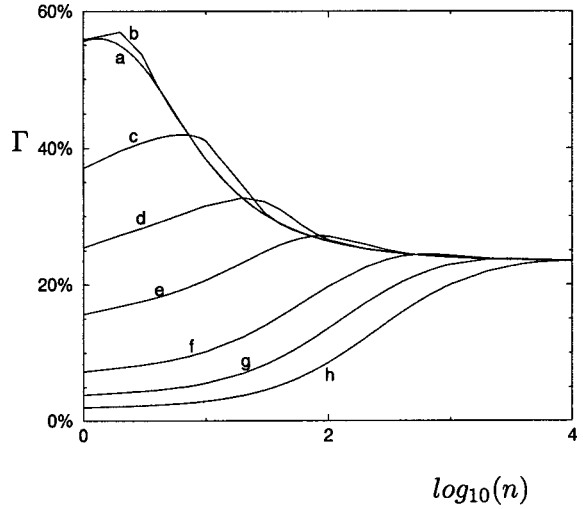

FIG. 5. Riga: The threshold reduction rate Γ vs $\log_{10}(n)$ for $s=q=1$ and different values of e/R. The labels correspond to those of Fig. 2.

expect the dissipation due to these eddy currents to be also maximum for $se'/R=O(1)$. However, in the case where the skin depth δ is smaller than e, we must replace e by δ in the expression of e'. Indeed, in the case where $\delta<e$, the dissipation is mainly concentrated in the skin layer. The skin depth is defined by $\delta/R=\sqrt{2/(ns\omega)}$ where ω is the dimensionless pulsation of the magnetic field that we also calculated solving Eq. (12). The curves for Riga are plotted in Fig. 4 (solid curves above the dotted curves and dashed curve at the top). For each thickness the maximum of Γ is indeed obtained at about the same value of $se'/R=O(1)$, followed by a sudden fall due to the additional eddy current dissipation. Increasing the wall conductivity helps the electric currents to close outside the fluid like in the stationary case. However, because of the skin effect (nonstationary solutions), increasing the wall conductivity prevents the magnetic field to close outside the fluid. It is the competition between these two effects which leads to the maximum of the threshold reduction rate Γ.

D. Influence of the wall permeability

1. Threshold reduction rate

In this section we vary the wall permeability n for $s=q=1$. We define again a threshold reduction rate by Eq. (19) in which s is replaced by n. The resulting reduction rates Γ for Riga and Karlsruhe are plotted, respectively, in Fig. 5 and Fig. 6 versus $\log_{10}(n)$ for different values of e/R. In the case of stationary solutions like for Karlsruhe, we find that Γ is monotonically increasing versus n. We explain this increase by a change of the geometry of the magnetic field lines in the fluid. When increasing n the field lines in the fluid become perpendicular to the wall. As a result they can close outside the fluid, decreasing the ohmic dissipation in the fluid. As a result the total dissipation decreases with n.

In the case of time-dependent solutions the dissipation due to the eddy currents must be added to the previous total dissipation. In that case, increasing the wall permeability still helps the magnetic field but prevents the electric currents from closing outside the fluid. This can explain the difference of slope between the curves a (negative slope) and h (positive slope) of Fig. 5. Indeed, in the case a the wall is probably larger than the skin depth and the eddy currents dissipate more than the reduction of dissipation due to the change of geometry of the field lines. In case h the wall is so small (smaller than the skin depth) that the additional dissipation due to the eddy currents is negligible.

A common feature of Riga and Karlsruhe is that $\Gamma(s,n=q=1)=\Gamma(n,s=q=1)$ for $e/R\to\infty$. Such a relation has already been found for the rigid body helical flow surrounded by a conducting layer of infinite extent [15].

For completeness we also calculated Γ when both s and n are changed (but still $q=1$). The corresponding curves are plotted in Fig. 7 for Riga ($e/R=86\%$) and in Fig. 8 for Karlsruhe ($e/R=0.1$).

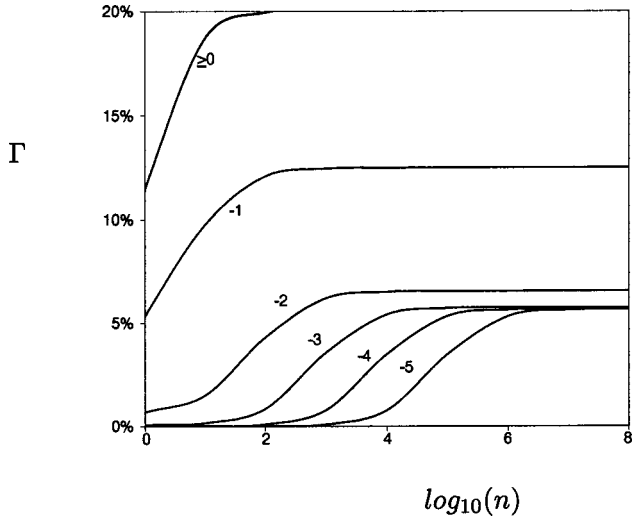

FIG. 6. Karlsruhe: The threshold reduction rate Γ vs $\log_{10}(n)$ for $s=q=1$ and different values of $\log_{10}(e/R)$ given by the labels.

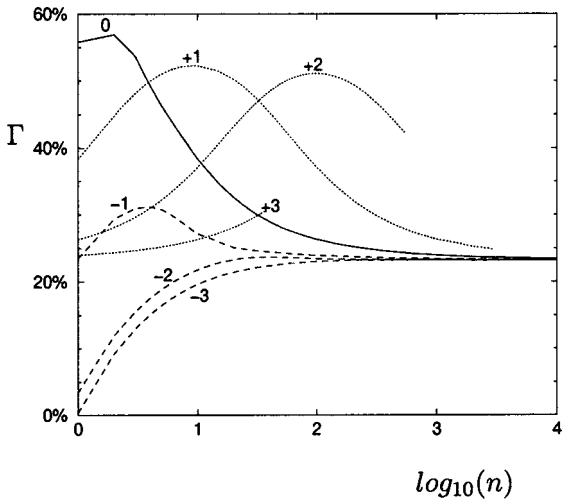

FIG. 7. Riga: The threshold reduction rate Γ vs $\log_{10}(n)$ for $e/R=86\%, q=1$, and different values of s. The labels correspond to $\log_{10}(s)$. The dotted (dashed) lines refer to positive (negative) values of $\log_{10}(s)$.

E. Influence of the fluid permeability

Here we look for the dynamo instability threshold assuming the use of a ferrofluid. The permeability of the wall is equal to the vacuum permeability. Therefore $s=n=1$ and $q=\mu_1/\mu_2$ is varied. A simple way to estimate the benefit of using a ferrofluid ($q>1$) is to assume that the dynamo instability threshold does not vary significantly from the case $q=1$. Then at the threshold $U(q)$ $[\alpha_\perp(q)]$ would behave like $U(q=1)/q$ $[\alpha_\perp(q=1)/q]$. Therefore the larger q is, the smaller U (or $\alpha_\perp$) would need to be, showing the possible benefit of using a ferrofluid. However, in this simple estimate the boundary conditions (10) in which the permeability jump between the fluid and the surrounding wall is considered, is not satisfied.

When solving the problem with the full boundary conditions (10) we find that, in fact, the threshold increases with q.

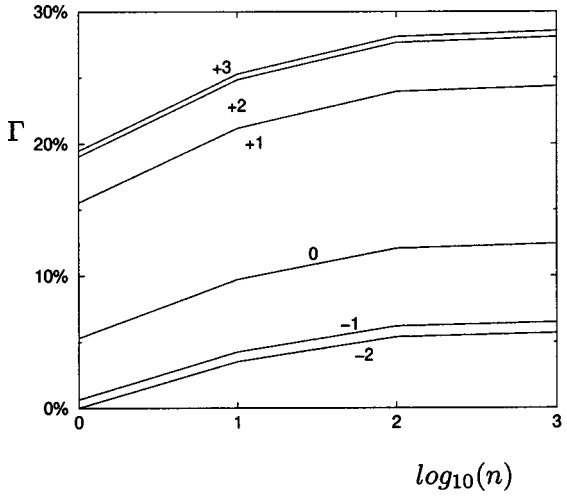

FIG. 8. Karlsruhe: The threshold reduction rate Γ vs $\log_{10}(n)$ for $e/R=0.1, q=1$, and different values of s. The labels correspond to $\log_{10}(s)$.

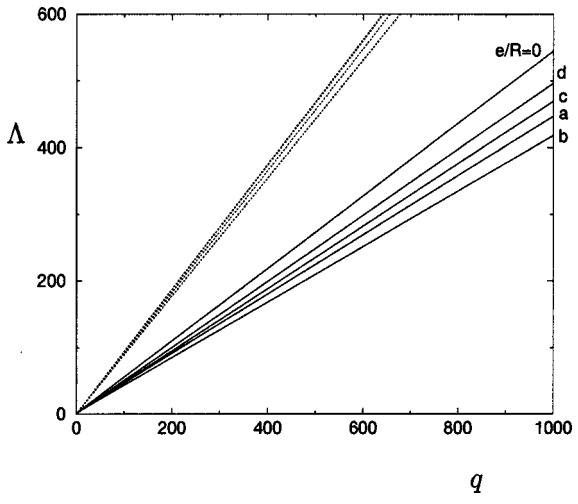

FIG. 9. The parameter Λ vs q for $n=s=1$ and different values of e/R. The solid (dotted) curves correspond to Riga (Karlsruhe). The labels correspond to those of Fig. 2.

As a result, using a ferrofluid is less interesting than suggested by the previous simple estimate. In order to quantify how much less interesting it is, we calculate $\Lambda=qR_m(q=1)/R_m(q)$ for Riga and $\Lambda=qR_\alpha(q=1)/R_\alpha(q)$ for Karlsruhe versus q. Then at the threshold $U(q)$ $[\alpha_\perp(q)]$ behaves like $U(q=1)/\Lambda$ $[\alpha_\perp(q=1)/\Lambda]$. The corresponding curves are plotted in Fig. 9 with solid (dotted) curves for Riga (Karlsruhe). We find that Λ is linear with q and that $1.8\leqslant q/\Lambda\leqslant 2.4$ for Riga and $1.06\leqslant q/\Lambda\leqslant 1.13$ for Karlsruhe. Finally, we conclude that using a ferrofluid is still interesting but again not as much as the simple previous estimate. Instead of being equal to q the gain on the flow intensity is about $q/2$ for Riga and $q/1.1$ for Karlsruhe.

V. CONCLUSION

For a dynamo laboratory experiment with stationary solutions, such as the Karlsruhe experiment, the addition of an external wall with a conductivity s larger than the fluid conductivity or with a permeability n larger than vacuum, leads to a reduction of the dynamo instability threshold. This reduction is monotonous with s and n. Typically the reduction can be as high as 20% when only s or n is increased and up to 28% when both are increased. This reduction is due to a change of geometry of the current lines or the magnetic field lines leading to a reduction of the total ohmic dissipation.

For a dynamo laboratory experiment with nonstationary solutions, such as the Riga experiment, the presence of some additional eddy currents in the external wall reminiscent to a skin effect changes the previous results. In particular, the reduction is not monotonous with s nor n. Indeed, the eddy currents produce an additional dissipation which can reduce the threshold drastically. As a result, there is an optimum conductivity s, permeability n, and wall thickness e/R for which the dynamo threshold is minimum. In Riga this optimum corresponds to a stagnant layer of liquid sodium ($s=n=1$) of thickness $e/R=86\%$. Besides, it is the value actually used for the Riga experiment.

Finally, the use of a ferrofluid with a relative permeability q times larger than the vacuum permeability is interesting because the gain on the velocity intensity or on the experiment dimension is about $q/2$ for Riga and $q/1.1$ for Karlsruhe. In practice, this could give some motivation for trying to obtain a ferrofluid with a permeability sufficiently large and homogeneous in space even in strong motion.

ACKNOWLEDGMENTS

R.A-Z. was supported by a Mexican CONACyT grant. Part of the coding was done by A.G. during a stay at the Laboratoire des Ecoulements Géophysiques et Industriels with support from the Institut National Polytechnique de Grenoble.

[1] A. Gailitis *et al.*, Phys. Rev. Lett. **84**, 4365 (2000).
[2] A. Gailitis, O. Lielausis, E. Platacis, S. Dementiev, A. Cifersons, G. Gerbeth, T. Gundrum, F. Stefani, M. Christen, and G. Will, Phys. Rev. Lett. **86**, 3024 (2001).
[3] R. Stieglitz and U. Müller, Phys. Fluids **13**, 561 (2001).
[4] P. Frick, S. Khripchenko, S. Denisov, J.-F. Pinton, and D. Sokoloff, Eur. Phys. J. B **25**, 399 (2002).
[5] A. Gailitis, O. Lielausis, E. Platacis, G. Gerbeth, and F. Stefani, Rev. Mod. Phys. **74**, 973 (2002).
[6] Magnetohydrodynamics **28** (1-2) (2002), special issue on MHD dynamo experiments, edited by K.-H. Rädler and A. Cebers.
[7] G. Roberts, Philos. Trans. R. Soc. London, Ser. A **271**, 411 (1972).
[8] K. Rädler, M. Rheinhardt, E. Apstein, and H. Fuchs, Nonlinear Processes in Geophysics **9**, 171 (2002).
[9] F. Krause and K.-H. Rädler, *Mean-Field Magnetohydrodynamics and Dynamo Theory* (Pergamon Press, New York, 1980).
[10] F. Plunian and K.-H. Rädler, Geophys. Astrophys. Fluid Dyn. **96**, 115 (2002).
[11] A. Gailitis, in *Topological Fluid Dynamics*, edited by H.K. Moffatt and A. Tsinober (Cambridge University Press, Cambridge, 1990).
[12] A. Gailitis and Y. Freiberg, Magnetohydrodynamics **16**, 11 (1980).
[13] R. Kaiser and A. Tilgner, Phys. Rev. E **60**, 2949 (1999).
[14] G. Sarson and D. Gubbins, J. Fluid Mech. **306**, 223 (1996).
[15] P. Marty, A. Ajakh, and A. Thess, Magnetohydrodynamics **30**, 474 (1995).